Silicon Oxy-Nitride for the Low Refractive Index Layers in the Mirror Coatings of the Cryogenic Laser Interferometer Gravitational Waves Detector

Shiuh Chao,* Wen-Jie Tsai, Dong-Lin Tsai, I-Peng Chang, Qian-Yi Hong, Wei-Chih Chang, and Yu-Hsun Kao
Institute of Photonics Technologies, National Tsing Hua University, Hsinchu 30013, Taiwan, Republic of China

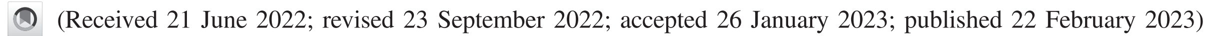

(Received 21 June 2022; revised 23 September 2022; accepted 26 January 2023; published 22 February 2023)

The low refractive index layers in the mirror coatings of the room-temperature laser interferometer gravitational waves detectors are silica deposited by the ion beam sputter method. However, the silica film suffers from the cryogenic mechanical loss peak, hindering its application for the next generation detector operated at cryogenics. New low refractive index materials need to be explored. We study amorphous silicon oxy-nitride (SiON) films deposited using the method of plasma-enhanced chemical vapor deposition. By changing the N_2O/SiH_4 flow rate ratio, we can tune the refractive index of the SiON smoothly from nitridelike to silicalike of ~1.48 at 1064 nm, 1550 nm, and 1950 nm. Thermal anneal reduced the refractive index down to ~1.46 and effectively reduced the absorption and cryogenic mechanical loss; the reductions correlated with the N─H bond concentration decrease. Extinction coefficients of the SiONs at the three wavelengths are reduced down to $5 \times 10^{-6} \sim 3 \times 10^{-7}$ by annealing. Cryogenic mechanical losses at 10 K and 20 K (for ET and KAGRA) of the annealed SiONs are significantly lower than the annealed ion beam sputter silica. They are comparable at 120 K (for LIGO-Voyager). Absorption from the vibrational modes of the N─H terminal-hydride structures dominates over the absorption from other terminal hydrides, the Urbach tail, and the silicon dangling bond states in SiON at the three wavelengths.

DOI: 10.1103/PhysRevLett.130.081403

Introduction.—Since the first detection of the gravitational waves by the LIGO-Virgo Collaboration in 2015 [1] and the successive detections of more than 90 gravitational wave events until the end of the third observation run [2], development for the next generation detectors is moving toward cryogenics operation to reduce the thermal noise for higher sensitivity [3,4]. Brownian coating thermal noise (CTN) is one of the primary noise sources for the detectors at the most sensitive range, around 100 Hz for LIGO-A^+ [3] and 60 Hz for LIGO-Voyager [4,5]. Brownian CTN is proportional to the mechanical loss angle of the coatings based on the fluctuation-dissipation theorem [6]. A stringent requirement on the absorption, at ~1 ppm level [3,7,8], for the mirror coatings is required as well to avoid thermal loading of the mirrors.

The dielectric mirror coatings are composed of a high refractive index layer (H) and a low refractive index layer (L). Each has a quarter-wave optical thickness and is stacked alternately to form the highly reflective multilayer coatings. CTN increases with total coating thickness; increasing the refractive index contrast between the H and L layers can effectively reduce the number of HL pairs required for a specific transmittance and reduce the CTN. The coating materials for current detectors operated at room temperature and 1064 nm wavelength are $Ti:Ta_2O_5$ for the H layer and silica for the L layer. Both were deposited by using the ion beam sputter (IBS) method [9,10] with good optical qualities and low room-temperature mechanical loss [11,12]. However, both materials have a mechanical loss peak at the cryogenics temperature range [13,14]; therefore, directly applying these materials to the coatings of the cryogenic detectors that were designed to operate at 10 K for the Einstein Telescope (ET) [7], 20 K for the KAGRA [8], and 120 K for the LIGO-Voyager [3] are hindered. There are reports for exploring new high refractive index films for the cryogenics coatings such as amorphous silicon (aSi), n ~ 3.4, [15] and amorphous silicon nitride (aSiN), n ~ 2.0–2.6, [16–18], but little on the low refractive index cryogenic coatings with a refractive index as low as that of silica.

Motivation.—The cryogenic mechanical loss peak of silica is believed to be due to the asymmetrical bond angles of the Si─O─Si in the amorphous SiO_2 network [19–21]. On the other hand, it was found that the cryogenic mechanical losses of the aSiN deposited by the chemical vapor deposition (CVD) method correlated positively with the N─H bond concentration and were relatively low and flat compared to that of the IBS silica [15]. Therefore, we were motivated in this study to break the structure of Si─O─Si partially in silica and replace it with Si─N─Si. In other words, to mix aSiN and SiO_2 to form the silicon oxy-nitride (SiON) to reduce the cryogenic mechanical loss and control the refractive index of the mixture as close to that of silica. Meanwhile, the absorption of SiON needs to

 © 2023 American Physical Society

be closely studied and kept as low as possible. This Letter reports the deposition method, results, and analyses emphasizing the refractive index and extinction coefficient and the cryogenic mechanical loss of the SiON films. The temperature and wavelength range of the studies are those for the ET, KAGRA, and LIGO-Voyager, i.e., 10 K, 20 K, and 120 K for the temperature and 1064 nm, 1550 nm, and 2000 nm for the wavelength, respectively [3,7,8].

Deposition.—Mirror coatings for the laser interferometer gravitational waves detectors used to date were deposited by the IBS method [9]. In this Letter, the SiON films were deposited using the plasma-enhanced chemical vapor deposition (PECVD) method. The advantage of the CVD coating is that a large area of uniform coatings is easier to achieve for the large mirror, ~45 cm in diameter, of the LIGO-Voyager and ET. In addition, the CVD method is more flexible in tuning the material composition than the IBS method by simply changing the reaction gases or the gas flow rate ratio rather than by changing the solid sputter targets. In our PECVD process for depositing SiON, the precursor gas was silane (SiH_4) and nitrous oxide (N_2O) with a carrier gas of N_2. By varying the N_2O/SiH_4 flow rate ratio from small to large, we tuned the composition of the films from nitridelike with higher refractive index and higher nitrogen content to silicalike with lower refractive index and higher oxygen content. The chemical formula of the film is expressed as $SiO_xN_yH_z$. The deposition parameters in our process were 1 Torr for the total pressure, 300 °C for the substrate temperature, 1500 sccm for the N_2 flow rate, and 20 W for the plasma-generating rf power.

Measurement.—The concentration of the terminal-hydride bonds N─H, Si─H, and O─H was measured by the Fourier transform IR spectroscopy; the detection limit was $\sim 10^{20}/\mathrm{cm}^3$. Silicon dangling bonds (DB, Si-) were measured by using the electron spin resonance with a detection limit of $\sim 10^{18}/\mathrm{cm}^3$. Atomic concentrations were measured by using x-ray photoelectron spectroscopy and deduced by the aids from the mass density measurement and the bond concentrations of the films. The exact measurements method and concentration deductions were carried out following the methods given in Ref. [16]. The refractive index at 1064 nm, 1550 nm, and 1950 nm thickness and energy band gap, i.e., the electronic mobility gap, were measured using the spectroscopic ellipsometer with the Tauc-Lorentz model [22]. Extinction coefficients at 1064 nm, 1550 nm, and 1950 nm were measured using the photothermal common-path interferometer [23].

The cryogenic mechanical loss was measured by measuring the ring-down time of a silicon cantilever double-side coated with the SiON films. The cantilever was clamped in a cryogenic chamber and excited at the resonant frequencies, and the mechanical loss angles of the coatings were deduced from the ring-down time. Details of the measurements and data deductions are also given in Ref. [16].

Results for the as-deposited films.—Samples were deposited with N_2O/SiH_4 flow rate ratios varied at 1, 3, 5, 9, 18, 27, and 90, respectively. Figure 1(a) shows the refractive index (@ 1064 nm, 1550 nm, and 1950 nm) and the band gap (Eg) vs N_2O/SiH_4 ratio. Figure 1(b) shows the atomic concentrations of Si, O, N, and H vs N_2O/SiH_4 ratio. It is clear that the films are changing smoothly from "nitridelike," i.e., higher refractive index, lower band gap, lower oxygen content, and higher nitrogen content, to "silicalike" with the parameters in reversed order from that of the nitridelike films. The refractive index at the three wavelengths is close and decreasing sharply from ~2.0 to ~1.48. The band gap increased from 2.40 eV up to approaching 6.85 eV. The chemical formula of the films changed from $SiO_{0.47}N_{0.21}H_{0.59}$ for ratio 1 to $SiO_{1.63}N_{0.02}H_{0.05}$ for ratio 90, as can be obtained from Fig. 1(b).

For the subsequent studies on the mechanical loss and annealing effect, we chose to study two films: the nitridelike film with flow rate ratio 3 ($SiO_{0.91}N_{0.27}H_{0.52}$, $n = 1.65$) and the silicalike film with flow rate ratio 27 ($SiO_{1.50}N_{0.04}H_{0.13}$, $n = 1.48$).

Cryogenic mechanical loss angles for four modes of these two samples are shown in Figs. 2(a) to 2(d), green for the silicalike and blue for the nitridelike samples, respectively. The red and orange curves are for the silica deposited by the standard PECVD process of the Taiwan Semiconductor Research Institute (TSRI) [24] and a silicon nitride deposited by PECVD published previously [17] for comparison purposes. The trend of the cryogenic mechanical loss changed from silica to silicalike, with a profound peak, to that of nitridelike and then to silicon nitride, with a lower and flatter loss curve.

Thermal annealing.—Annealing is an effective method to reduce the mechanical loss of IBS silica and $Ti:Ta_2O_5$ [25,26]. For the silicalike sample shown in Fig. 2, the Si─H bond density was low, 4×10^{20}, and the band gap was high at 5.92 eV; the absorption so produced by the excessive silicon DB created by the annealing should be limited and inhibited by the large band gap. Therefore, we chose to anneal the silicalike SiON at a high temperature of 900 °C. On the other hand, the nitridelike SiON has a higher Si─H bond density,

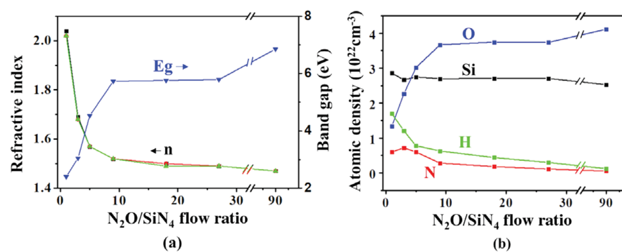

FIG. 1. (a) Refractive index n at 1064 nm (green), 1550 nm (red), 1950 nm (black), band gap (Eg). (b) Concentrations of O, Si, H, and N vs N_2O/SiH_4 flow rate ratio.

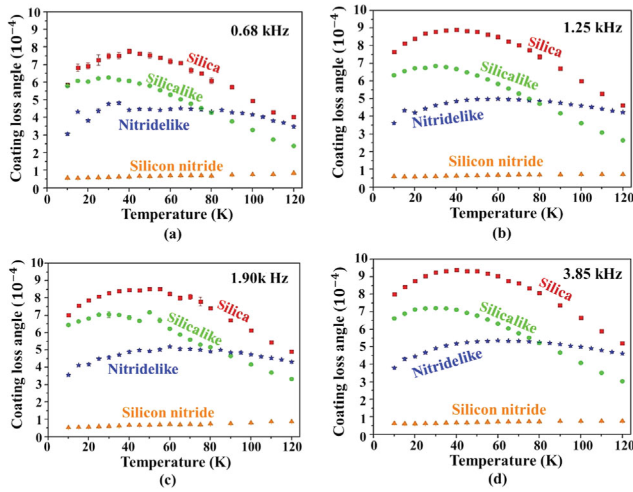

FIG. 2. Cryogenic mechanical loss angle of the silicalike SiON (green), the nitridelike SiON (blue), the TSRI standard silica (red), and the silicon nitride (orange) at four different frequencies: (a) 0.68 kHz, bending mode; (b) 1.25 kHz, torsion mode; (c) 1.90 kHz, bending mode; and (d) 3.85 kHz, torsion mode.

1.22×10^{22}, and a lower band gap, 3.09 eV; therefore, we chose to anneal the nitridelike SiON at a lower temperature of 500 °C.

Annealing results for the nitridelike SiON.—As shown in Figs. 3(a) and 3(b), the variations of the refractive index at the three wavelengths and the band gaps are relatively small, while the variations of the extinction coefficients at the three wavelengths, the DB concentration, and the N─H bond concentrations dropped drastically during the first hour of annealing and the variations are well-correlated. The lowest extinction coefficients for the three wavelengths through annealing are 1.05×10^{-6} at 1064 nm, 2.88×10^{-6} at 1550 nm, and 4.85×10^{-6} at 1950 nm.

The cryogenic mechanical loss angle of the four modes for the nitridelike sample annealed at 500 °C for 6 h is shown in Fig. 3(c), together with that of the as-deposited from Fig. 2. It is clear that a significant reduction in loss angle was obtained through 500 °C annealing.

Annealing results for the silicalike.—As shown in Figs. 4(a) and 4(b), the refractive index at three wavelengths dropped down from ∼1.48 to ∼1.46, close to that of silica. Extinction coefficients dropped down to the low end of 10^{-6} at 1950 nm and into the low end of 10^{-7} at 1550 nm and 1064 nm. The band gap remained relatively constant, the N─H bond dropped from 0.35×10^{22} to 0.02×10^{22}, and the DB increased and then decreased with the increasing annealing time. Variation of the extinction coefficients correlated with the N─H bonds but not with the DB. The lowest extinction coefficients of the annealed samples are 3.3×10^{-7} at 1064 nm, 5.8×10^{-7} at 1550 nm, and 2.6×10^{-6} at 1950 nm.

Cryogenic mechanical loss angle of four modes annealed at 900 °C for 6 h is shown in Fig. 4(c) together with that of the as-deposited from Fig. 2. It is clear that the loss angle was reduced significantly through 900 °C annealing.

Absorption mechanisms.—Vibration modes of the terminal-hydride structure in SiON, i.e., O─H, Si─H,

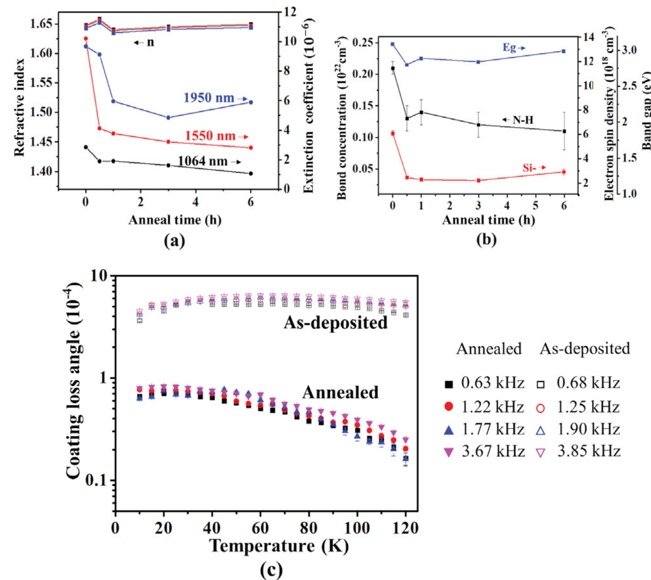

FIG. 3. Annealing results of the nitridelike SiON. (a) Refractive index and extinction coefficients at 1064 nm, 1550 nm, and 1950 nm. (b) Band gap, silicon dangling bond, and N─H bond concentrations vs annealing time at 500 °C. (c) Cryogenic mechanical loss of the four modes for the as-deposited and the annealed.

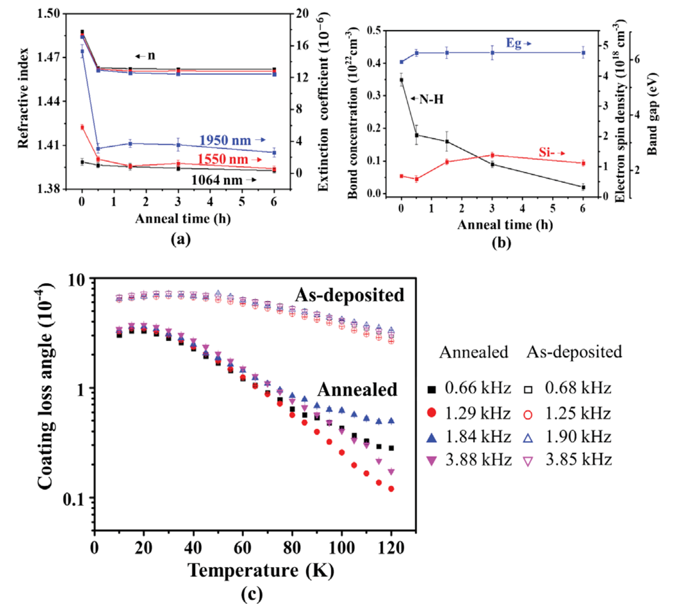

FIG. 4. Annealing results of the silicalike SiON. (a) Refractive index and extinction coefficients at 1064 nm, 1550 nm, and 1950 nm. (b) Band gap, silicon dangling bond, and N─H bond concentrations vs annealing time at 900 °C. (c) Cryogenic mechanical loss of the four modes for the as-deposited and the annealed.

and N—H, may contribute to the absorption at the three wavelengths of interest. For the O—H bond, stretching mode exists at $\sim 3600\ \mathrm{cm}^{-1}$ (2.78 μm) [27,28]; the fundamental and its overtones do not cover any of the three wavelengths. For the Si—H bond, resonant frequencies and their overtones (up to the second overtone) of all the vibration modes are mostly in the mid-IR [29]; only the second overtone of the stretching modes of $-$SiH, $-SiH_2$, and $-SiH_3$, at $\sim 2180\ \mathrm{cm}^{-1}$ (4.59 μm) [30,31], are near 1550 nm. For the N—H bond, the stretching modes of N—H and $N—H_2$ are in the vicinity of $\sim 3300\ \mathrm{cm}^{-1}$ (3.03 μm) [28,30] and extended to $\sim 2900\ \mathrm{cm}^{-1}$ (3.45 μm) by the hydrogen bonding between the H in the N—H bond and lone-pair electron on nearby N atoms [30,32], the first overtone of which covers the 1550 nm and the second overtone covers the 1064 nm. In addition, the fundamental frequency of the combination modes of $N—H_2$ (stretching plus bending) is in the vicinity of $\sim 5050\ \mathrm{cm}^{-1}$ (1.98 μm) [33,34], which covers 1950 nm and up to 2000 nm. Since the absorption strength of the vibration modes should be the strongest for the wavelength that coincides with the fundamental resonance and weaker with the first overtone and then the second overtone; therefore, we can qualitatively conclude that, first, the vibration modes of the N—H structures dominate the absorption of the terminal hydrides in SiON, and second, among the absorption by the various N—H modes at the three wavelengths, absorption at 1950 nm is the highest due to the fact that the absorption comes from the fundamental resonance of an N—H mode; absorption at 1550 nm is the second highest that includes the first overtone resonance, and absorption at 1064 nm is the lowest that comes from only the second overtone resonance. This argument is qualitatively consistent with the observed order of the N—H dependent absorption level between the three wavelengths, as shown in Figs. 3(a) and 3(b) and Figs. 4(a) and 4(b).

Photon-induced electronic transition in the Urbach-tail states [35–37] of the amorphous material in general and silicon dangling bonds (DB) in the hydrogenated amorphous silicon [38] also contributes to optical absorption in amorphous semiconductors. The neutral dangling bond state lies in the middle of the band gap with the positive and negative charged DB states closely spaced in energy [39]; therefore, the absorption strength of the DB in the near IR is smaller for larger band gap materials than for smaller band gap materials, e.g., silica vs amorphous silicon. Therefore, for the silicalike SiON with band gap ~ 5.8 eV and ~ 6.26 eV before and after annealing, Fig. 4(b), the DB is likely to contribute insignificantly to absorption. The Urbach absorption is known to follow a linear exponential photon-energy dependence [37], while another linear exponential photon-energy dependent function [38,39] describes the DB absorption at lower photon energy and with a smaller slope than the Urbach tail. Both absorptions increase with increasing photon energy. However, the order of the absorption levels among the three wavelengths in Figs. 3 and 4 is opposite to this trend but rather consistent with that of the N—H-dependent absorption as previously discussed. This implies that the absorption of SiON at the level of our observation is dominated by the vibrational modes of the N—H terminal-hydride structures rather than the absorption from the electronic transitions of the Urbach-tail and DB states.

Mechanical loss mechanism.—The mechanical loss of silica glass is known to have a peak at cryogenics temperature, attributed to thermally activated switching between two asymmetrical Si—O—Si bond angles [18,19] and the associated rotation of a group of atoms [19]. An asymmetrical double-well potential model (a two-level system) is commonly accepted and used to analyze the phenomenon [40]. The broadened peak in the silica thin films reflects a wide distribution of the related parameters in the glassy state, such as the bond angle, asymmetry of the double well, and activation energy. The peak narrowing and reduction upon thermal anneal [25] imply a narrowing in the distribution of the related parameters. On the other hand, for the amorphous silicon nitride deposited by the PECVD process, a lower and flatter loss distribution was observed, and the cryogenic loss angle correlated positively with the N—H bond concentration [16]. It was then postulated that the switching between the position of the H^+ and the lone-pair electron associated with the N—H bonds by phonon-assisted tunneling is counted for the loss mechanism. It is expected that decreasing N—H concentration through thermal annealing should reduce the cryogenic mechanical loss of SiN. Trends in Figs. 2, 3(c), and 4(c) suggest that the loss mechanism in the as-deposited and the annealed SiON should contain contributions from that of silica and SiN and some combined mechanisms that are to be explored; the narrowing and reduction of the loss angle in Fig. 4(c)

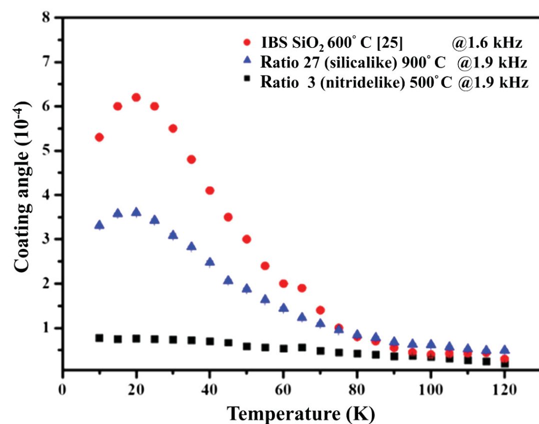

FIG. 5. Cryogenic mechanical loss of 600 °C annealed IBS silica at 1.6 kHz [25] (red), 900 °C annealed silicalike SiON at 1.9 kHz (blue), and 500 °C annealed nitridelike SiON at 1.9 kHz (black).

TABLE I. Comparison of the refractive index, extinction coefficients (at 1064 nm, 1550 nm, and 1950 nm), and cryogenic mechanical loss (at 10 K, 20 K, and 120 K) for the IBS-silica with anneal, silicalike SiON with anneal, and nitridelike SiON with anneal.

	Refractive index			Extinction coefficient (10^{-7})			Cryogenic mechanical loss (10^{-4})		
Material	1064 nm	1550 nm	1950 nm	1064 nm	1550 nm	1950 nm	10 K	20 K	120 K
IBS SiO_2 with anneal	1.44 ~ 1.47 [12,44]	1.44 ~ 1.46 [12]	NA	0.36 [45]	0.8 [41]	NA	5.3 [25]	6.2 [25]	0.3 [25]
SiON (ratio 27 silicalike)	1.4621	1.4609	1.4588	3.30 ± 1.67	5.80 ± 3.21	26.0 ± 5.72	3.31 ± 0.01	3.60 ± 0.02	0.49 ± 0.01
SiON (ratio 3 nitridelike)	1.6496	1.6478	1.6439	10.5 ± 1.65	28.8 ± 2.43	48.5 ± 6.61	0.63 ± 0.05	0.75 ± 0.05	0.16 ± 0.04

implies that the dominant loss mechanism in the silicalike SiON should be that of the two-level system origin of the silica, and the large reduction with the relatively flat loss distribution in Fig. 3(c) implies that the dominant loss mechanism in the nitridelike SiON should be the N─H related as was postulated.

Comparison and conclusion.—Figure 5 and Table I show the comparison of the annealed IBS silica [25] with the annealed silicalike SiON and the annealed nitridelike SiON. The loss angle is compared for the similar frequency at 1.9 kHz and 1.6 kHz. First, a refractive index of ~1.46 for the SiON, close to that of silica, is achievable. Second, for ET and KAGRA at 10 K and 20 K, the mechanical loss of the SiONs is significantly lower than that of the IBS silica and comparable to the IBS silica for LIGO-Voyager at 120 K. Third, the absorption of the SiONs is in the range of mid-10^{-6} to the low end of 10^{-7} for the three wavelengths, higher than that of the IBS silica. It is concluded that N─H bonds are the major sources of absorption. Methods for further reducing the N─H bonds, such as higher temperature or prolonged annealing, high temperature-low deposition rate CVD, such as the low-pressure CVD, are plausible. Multimaterial configurations [41–43] containing both SiON and silica for low mechanical loss and low absorption mirror coatings could be adopted for the next-generation cryogenic detectors. The H-free IBS deposition method is an alternative method to deposit SiON films, although not trivial. One of the difficulties for the IBS is to prepare the sizeable solid sputter target with the correct composition, and our results on the optimal SiON films could help solve the problem.

The authors are grateful for using the sample fabrication facilities provided by the Taiwan Semiconductor Research Institute (TSRI). Acknowledgment of the financial support goes to the Ministry of Science and Technology (MOST) of Taiwan under Contract No. 110-2221-E-007-088. The authors are grateful for the reviews and comments from the Optics Working Group of the LIGO Scientific Collaboration.

*Corresponding author.
schao@ee.nthu.edu.tw

[1] B. P. Abbott *et al.* (LIGO Scientific and Virgo Collaborations), Observation of Gravitational Waves from a Binary Black Hole Merger, Phys. Rev. Lett. **116**, 061102 (2016).
[2] R. Abbott *et al.*, GWTC-3: Compact binary coalescences observed by LIGO and Virgo during the second part of the third observing run, arXiv:2111.03606.
[3] LIGO Scientific Collaboration, Instrument Science White Paper Report No. LIGO-T1600119-v4, 2016.
[4] LIGO Scientific Collaboration, Instrument Science White Paper Report No. LIGO-T2100298-v2, 2021.
[5] R. X. Adhikari *et al.*, A cryogenic silicon interferometer for gravitational-wave detection, Classical Quantum Gravity **37**, 165003 (2020).
[6] H. B. Callen and T. A. Welton, Irreversibility and generalized noise, Phys. Rev. **83**, 34 (1951).
[7] M. Abernathy, F. Acernese, and P. Ajith, Einstein gravitational wave Telescope conceptual design study: Report No. ET-0106C-10, 2011.
[8] K. Somiya, Detector configuration of KAGRA-the Japanese cryogenic gravitational-wave detector, Classical Quantum Gravity **29**, 124007 (2012).
[9] L. Pinard *et al.*, Mirrors used in the LIGO interferometers for first detection of gravitational waves, Appl. Opt. **56**, C11 (2017).
[10] J. Aasi *et al.* (LIGO Scientific Collaboration), Advanced LIGO, Classical Quantum Gravity **32**, 074001 (2015).
[11] G. M. Harry *et al.*, Titania-doped tantala/silica coatings for gravitational-wave detection, Classical Quantum Gravity **24**, 405 (2007).
[12] M. Granata *et al.*, Amorphous optical coatings of present gravitational-wave interferometers, Classical Quantum Gravity **37**, 059004 (2020).
[13] I. W. Martin *et al.*, Comparison of the temperature dependence of the mechanical dissipation in thin films of Ta_2O_5 and Ta_2O_5 doped with TiO_2, Classical Quantum Gravity **26**, 155012 (2009).
[14] I. W. Martin *et al.*, Low temperature mechanical dissipation of an ion-beam sputtered silica film, Classical Quantum Gravity **31**, 035019 (2014).
[15] P. G. Murray, I. W. Martin, K. Craig, J. Hough, R. Robie, S. Rowan, M. R. Abernathy, T. Pershing, and S. Penn,

Ion-beam sputtered amorphous silicon films for cryogenic precision measurement systems, Phys. Rev. D **92**, 062001 (2015).

[16] H. W. Pan, L. C. Kuo, S. Y. Huang, M. Y. Wu, Y. H. Juang, C. W. Lee, H. C. Chen, T. T. Wen, and S. Chao, Silicon nitride films fabricated by a plasma-enhanced chemical vapor deposition method for coatings of the laser interferometer gravitational wave detector, Phys. Rev. D **97**, 022004 (2018).

[17] D. S. Tsai, Z.-L. Huang, W.-C. Chang, and S. Chao, Amorphous silicon nitride films fabricated by an NH_3-free plasma enhanced chemical vapor deposition method with low cryogenic mechanical loss for the coatings of the next generation laser interferometer gravitational waves detector, Classical Quantum Gravity **39**, 15LT01 (2022).

[18] M. Granata *et al.*, Progress in the measurement and reduction of thermal noise in optical coatings for gravitational-wave detectors, Appl. Opt. **59**, A229 (2020).

[19] O. L. Anderson and H. E. Bommel, Ultrasonic Absorption in fused silica at low temperatures and high frequencies, J. Am. Ceram. Soc. **38**, 125 (1955).

[20] W. A. Phillips, Two-level states in glasses, Rep. Prog. Phys. **50**, 1657 (1987).

[21] R. Hamdan, J. P. Trinastic, and H. P. Cheng, Molecular dynamics study of the mechanical loss in amorphous pure and doped silica, J. Chem. Phys. **141**, 054501 (2014).

[22] G. E. Jellison Jr. and F. A. Modine, Parameterization of the optical functions of amorphous materials in the interband region, Appl. Phys. Lett. **69**, 371 (1996).

[23] A. Alexandrovski, W. Andrew Clarkson, N. Hodgson, M. Fejer, A. Markosian, R. K. Shori, and R. Route, Photothermal common-path interferometry (PCI): New developments, Proc. SPIE Int. Soc. Opt. Eng. **7193**, 71930D1 (2009).

[24] Taiwan Semiconductor Research Institute standard PECVD recipe for silica (private communication).

[25] R. Robie, Characterisation of the mechanical properties of thin-film mirror coating materials for use in future interferometric gravitational wave detectors, Ph.D. thesis. University of Glasgow, 2018.

[26] I. W. Martin *et al.*, Effect of heat treatment on mechanical dissipation in Ta_2O_5 coating, Classical Quantum Gravity **27**, 225020 (2010).

[27] B. A. Morrow and A. J. McFarlan, Surface vibrational modes of silanol groups on silica, J. Phys. Chem. **96**, 3 (1992).

[28] F. Ay and A. Aydinli, Comparative investigation of hydrogen bonding in silicon based PECVD grown dielectrics for optical waveguides, Opt. Mater. **26**, 1 (2004).

[29] M. H. Srodsky, M. Cardona, and J. J. Cuomo, Infrared and Raman spectra of the silicon-hydrogen bonds in amorphous silicon prepared by glow discharge and sputtering, Phys. Rev. B **16**, 3556 (1977).

[30] Z. Yin and F. W. Smith, Optical dielectric function and infrared absorption of hydrogenated amorphous silicon nitride films: Experimental results and effective-medium-approximation analysis, Phys. Rev. B **42**, 3666 (1990).

[31] J. Viard *et al.*, Si─H bonding environment in PECVD a-SiOxNy: H thin films, J. Eur. Ceram. Soc. **17**, 2029 (1997).

[32] L, Qing *et al.*, Vertertical integration of silicon nitride on siliconon-insulator platform, in *The 9th International Conference on Group IV Photonics (GFP)* (IEEE, New York, 2012).

[33] J. H. FU and J. R. Schlup, Mid- and near-infrared spectroscopic investigations of reactions between phenyl glycidyl ether (PGE) and aromatic amines, J. Appl. Polym. Sci. **49**, 2 (1993).

[34] K. B. Whetsel, W. E. Roberson, and M. W. Krell, Near-infrared spectra of primary aromatic amines, Anal. Chem. **30**, 10 (1958).

[35] F. Urbach, The long-wavelength edge of photographic sensitivityand of the electronic absorption of solids, Phys. Rev. **92**, 1324 (1953).

[36] W. Martienssen, The optical absorption edge in ionic crystals, Phys. Chem. Solids **2**, 257 (1957).

[37] H. Sumi and A. Sumi, The Urbach-Martienssen rule revisited, J. Phys. Soc. Jpn. **56**, 2211 (1987).

[38] B. J. Warren and N. M. Amer, Direct measurement of gap-state absorption in hydrogenated amorphous silicon by photothermal deflection spectroscopy, Phys. Rev. B **25**, 8 (1982).

[39] J. Singh and K. Shimakawa, *Advances in Amorphous Semiconductors* (Taylor & Francis, London, 2003), ISSN 0-415-28770-7.

[40] K. S. Gilroy and W. A. Philli, An asymmetric double-well potential model for structural relaxation processes in amorphous materials, Philos. Mag. B **43**, 5 (1981).

[41] K. Craig *et al.*, Mirror Coating Solution for the Cryogenic Einstein Telescope, Phys. Rev. Lett. **122**, 231102 (2019).

[42] J. Steinlechner, I. W. Martin, J. Hough, C. Kruger, S. Rowan, and R. Schnabel, Thermal noise reduction and absorption optimization via multimaterial coatings, Phys. Rev. D **91**, 042001 (2015).

[43] H. W. Pan *et al.*, Silicon nitride and silica quarter-wave stacks for low-thermal-noise mirror coatings, Phys. Rev. D **98**, 102001(2018).

[44] M. A. Fazio, G. Vajente, L. Yang, A. Ananyeva, and C. S. Menoni, Comprehensive study of amorphous metal oxide and Ta_2O_5-based mixed oxide coatings for gravitational-wave detectors, Phys. Rev. D **105**, 102008 (2022).

[45] C. Comtet *et al.*, Reduction of tantala mechanical losses in Ta_2O_5/SiO_2 coatings for the next generation of Virgo and LIGO interferometric gravitational waves detectors, *42nd Rencontres de Moriond Gravitational Waves and Experimental Gravity* (HAL Open Science, 2007).